Available online at www.sciencedirect.com
ScienceDirect
Journal of Power Sources 158 (2006) 1290–1305
JOURNAL OF POWER SOURCES
www.elsevier.com/locate/jpowsour

Evaluation of system configurations for solid oxide fuel cell-based micro-combined heat and power generators in residential applications

R.J. Braun *, S.A. Klein, D.T. Reindl

Mechanical Engineering Department, University of Wisconsin-Madison, 1500 Engineering Drive, Madison, WI 53706, USA

Received 20 May 2005; received in revised form 15 October 2005; accepted 17 October 2005
Available online 29 November 2005

Abstract

The evaluation of solid oxide fuel cell (SOFC) combined heat and power (CHP) system configurations for application in residential dwellings is explored through modeling and simulation of cell-stacks including the balance-of-plant equipment. Five different SOFC system designs are evaluated in terms of their energetic performance and suitability for meeting residential thermal-to-electric ratios. Effective system concepts and key performance parameters are identified. The SOFC stack performance is based on anode-supported planar geometry. A cell model is scaled-up to predict voltage–current performance characteristics when served with either hydrogen or methane fuel gas sources. System comparisons for both fuel types are made in terms of first and second law efficiencies. The results indicate that maximum efficiency is achieved when cathode and anode gas recirculation is used along with internal reforming of methane. System electric efficiencies of 40% HHV (45% LHV) and combined heat and power efficiencies of 79% (88% LHV) are described. The amount of heat loss from small-scale SOFC systems is included in the analyses and can have an adverse impact on CHP efficiency. Performance comparisons of hydrogen-fueled versus methane-fueled SOFC systems are also given. The comparisons indicate that hydrogen-based SOFC systems do not offer efficiency performance advantages over methane-fueled SOFC systems. Sensitivity of this result to fuel cell operating parameter selection demonstrates that the magnitude of the efficiency advantage of methane-fueled SOFC systems over hydrogen-fueled ones can be as high as 6%.

Keywords: Solid oxide fuel cells; Combined heat and power; System design; Exergy analysis; Residential fuel cell systems; Hydrogen

1. Introduction

The entry of fuel cell technology into the stationary power marketplace has the potential to increase energy conversion efficiencies and substantially reduce energy-related emissions associated with the residential energy sector. Micro-combined heat and power (micro-CHP) technologies, such as fuel cells and stationary engines, offer higher overall efficiencies than current central power plants and are gradually becoming economically viable as distributed generation resources [1]. Although fuel cells themselves have been studied extensively, a considerable gap exists in the area of application techniques to maximize benefits of fuel cell *systems* for both electrical energy generation and thermal energy utilization.

Design studies for stationary fuel cell systems have been receiving increased attention [2–4]. The principal focus of previous studies has been on fuel cell systems of larger capacities (200–500 kW) or on SOFC systems that are integrated with gas turbine cycles (e.g., [5,6]). In this paper, we explore several system configurations that aim to achieve optimal performance for solid oxide fuel cell systems in small-scale (1–10 kW) combined heat and power applications, with particular emphasis on application toward single-family detached dwellings. The study is carried out through simulation of various SOFC energy system configurations using previously developed and validated modeling tools [7]. This paper begins with a brief synopsis of the SOFC system model developed. System efficiency metrics and select operating parameters are defined next. Requirements in the form of thermal-to-electric load profiles are then discussed for typical single-family residential dwellings. Because of the growing interest in establishing a hydrogen economy, we evaluate performance differences between hydrogen-fueled SOFC systems and those directly supplied with natu-

* Corresponding author. Present address: United Technologies Research Center, 411 Silver Lane, E. Hartford, CT 06108, USA. Tel.: +1 860 610 7020; fax: +1 860 660 8329.
E-mail address: braunrj@utrc.utc.com (R.J. Braun).

0378-7753/$ – see front matter © 2005 Elsevier B.V. All rights reserved.
doi:10.1016/j.jpowsour.2005.10.064

Nomenclature

a	Tafel parameter, specific exergy
$\dot{A}$	exergy flow rate
AC	ac power
AGR	anode gas recycle
b	Tafel parameter
CGR	cathode gas recycle
DC	dc power
E	ideal voltage
$\dot{E}$	exergy flow rate
ER	external reforming
F	Faraday's constant or fuel cost
FPS	fuel processing subsystem
HHV	higher heating value
i	current
IR	internal reforming
LHV	lower heating value
n	number of electrons
$\dot{n}$	molar flow rate
p	pressure
P	power
$\dot{q}$, $\dot{Q}$	heat flow rate
R	universal gas constant, cell resistance, or capital recovery factor
T	temperature
U	utilization
UA	heat exchanger performance characteristic
V	cell voltage

Greek letters

δ	thickness of cell tri-layer
η	efficiency
λ	amount of excess air

Subscripts

as	anode limiting
e	electric
f	fuel
H	heating
II	second law
j	species
mech	mechanical
N	Nernst
PCS	power conditioning subsystem
s	solid
sys	system
U	universal gas

ral gas. A range of system concepts are evaluated on both first and second law efficiency bases for both hydrogen- and methane-fueled systems. The performance of these alternative fuel options is then compared. The paper concludes with a summary and final comments regarding successful application of the technology.

2. SOFC system modeling

The SOFC-CHP systems consist of pumping devices (blowers, ejectors, compressor, and water pump), gas-to-gas and gas-to-liquid heat exchangers, the fuel cell stack, fuel processing hardware (desulfurizer and reformer), catalytic combustor, and power conditioning device. Component models capable of accurately predicting the performance of the fuel cell stack, reformer, and remaining balance-of-plant (BOP) were implemented. A basic thermodynamic approach using a single-node (i.e., zero dimensional) steady-state model is used for each of the system components with the exception of the solid oxide fuel cell-stack.

2.1. Balance-of-plant models

Each model is made up of a system of governing equations, the formulation of which is derived from: (1) boundary conditions, (2) conservation laws, (3) property relations, and (4) performance characteristics of the component. Mass and energy balances are written for each component in the system. Performance characteristics, such as blower and compressor efficiency maps and cell-stack voltage–current characteristics are included in the models. Air blower and fuel compressor isentropic efficiencies were set to 62.5 and 70%, respectively. The inverter was assumed to have an efficiency of 92% based on manufacturer's data [8]. These models were integrated to generate a system of non-linear equations which were solved simultaneously using a general-purpose equation solver [9], thereby providing all the state point variables in the system. A detailed description of the models can be found in [7].

The system pressure drop varied with each configuration depending on the number of components within the system. Component pressure drops were estimated from a survey of the literature [3,10,11]. The air-side pressure drop ranged from 300 mbar (hydrogen-fueled) to 315 mbar (natural gas-fueled). Fuel-side pressure drop ranged from 210 mbar (hydrogen) to 335 mbar (natural gas). The required blower or compressor pressure rise is sensitive to the amount of recycle employed in ejector systems. A simple ejector model that employs a specified ejector efficiency establishes the amount of driving pressure required for a specified amount of entrained flow. Details on ejector efficiency and performance are provided in a subsequent section. A summary of the fuel reformer and fuel cell stack component models is provided below.

2.2. Fuel reformer

The reformer is a packed bed reactor integrating the fuel preheating and pre-reforming processes. Three processes are modeled in the reformer: (1) preheat of fuel-steam mixture to the desired pre-reformer temperature; (2) partial conversion of methane; and (3) water-gas shift equilibration. For steady-state system simulation of the reformer throughout the operating range, a zero-dimensional model incorporating chemical equilibrium calculations is employed. The extent of methane conversion is specified and the resulting reactor product gas determined by using water-gas shift equilibrium on the

remaining gas constituents. This method of determining reactor product gas composition was found to be in good agreement with the method of Gibbs energy minimization for 100% methane conversion [7]. At present, an equilibrium routine is sufficient for steady-state simulation objectives as the reformate composition of small pre-commercial reformers operating at design load is very near the equilibrium composition [12].

2.3. SOFC stack model

A steady-state, one-dimensional, cell-level model capable of resolving spatial distributions of temperature, composition, and current was developed. Separate material and energy balances on the gaseous fuel and air compartments, solid tri-layer, and the metallic interconnect were made on a discretized unit cell as shown in Fig. 1 to simulate the physicochemical processes in the gas channel.

The one-dimensional model assumes the reactant gas streams are parallel to one another. In a strict sense, this assumption limits the results to SOFC designs in which the reactant gas streams are in co-flow or counter-flow configurations (i.e., no cross-flow). The one-dimensional approach was considered sufficient for the purposes of this study as power, voltage, and outlet gas temperature predictions for cross-flow typically fall between co- and counter-flow configuration results [13]. A uniform distribution of feed gases to each individual cell in the stack and among the channels in each cell has also been assumed. This assumption has been made as the results of the present effort are aimed at characterizing the performance of optimized commercial cell-stack designs for system-level analyses. Furthermore, while maldistribution of the reactant gases within the stack can result in under-predictions of about 15% in solid temperature and current density gradients, it has been shown that these non-uniformities are insignificant in predicting cell voltage and power [14]. The temperature of the solid cell structure (anode-electrolyte-cathode) is assumed to be spatially uniform (i.e., lumped). The lumped temperature assumption for thin cell structures was validated by the work of Ackermann et al., [15] who showed that the cross-plane temperature difference in the heterogeneous cell structure is less than 1 °C for internally reforming SOFCs.

The reaction chemistry modeled within the cell includes steam reformation of methane, water-gas shift, and electrochemical oxidation of hydrogen, as well as ionic transport of oxygen across the electrolyte. The kinetics of internal steam reforming of methane over nickel cermet anode surfaces were based on the work of Achenbach and Riensche [16]. Energy balances include conduction, convection, and cross-channel radiation heat transfer mechanisms coupled to the heat generation associated with the reforming, water-gas shift, and electrochemical oxidation reactions on the anode layer. The resultant model is sensitive to variations in cell voltage, operating temperature, reactant utilization, and reactant composition.

The cell voltage–current performance characteristic is generated using the form of Kim et al. [17],

$$V(i) = E_{\mathrm{N}}(T, p_j) - \underbrace{iR_{\mathrm{cell}}(T_{\mathrm{s}})}_{\text{ohmic polarization}} - \underbrace{[a + b\ln(i)]}_{\text{activation polarization}} + \underbrace{\frac{R_{\mathrm{u}}T_{\mathrm{s}}}{2F}\left[\ln\left(1 - \frac{i}{i_{\mathrm{as}}}\right) - \ln\left(1 + \frac{p^0_{\mathrm{H_2}} i}{p^0_{\mathrm{H_2O}} i_{\mathrm{as}}}\right)\right]}_{\text{concentration polarization}} \quad (1)$$

where E_{N} is the Nernst potential, i is the cell current density, R_U the universal gas constant, T_{s} the cell temperature, a and b are Tafel parameters, R_{cell} is the total cell resistance, i_{as} is the limiting current density at the anode electrode, and p^o_j is the partial pressure of species j in the bulk flow. The advantage of this V–I representation is that it provides four physically meaningful parameters (R_{cell}, i_{as}, a, and b) that can be fit to experimental data. These parameters are determined from published manufacturer performance data [18] for a single-cell, anode-supported design using an yttria-stabilized zirconia electrolyte and a metallic interconnect as shown in Fig. 2(a). Fig. 2(b) depicts a voltage–current and power density comparison of hydrogen- and methane-fueled SOFCs. The model was validated with a benchmark sponsored by the International Energy Agency [13]. Additional details of the SOFC model development and its validation are documented in [7].

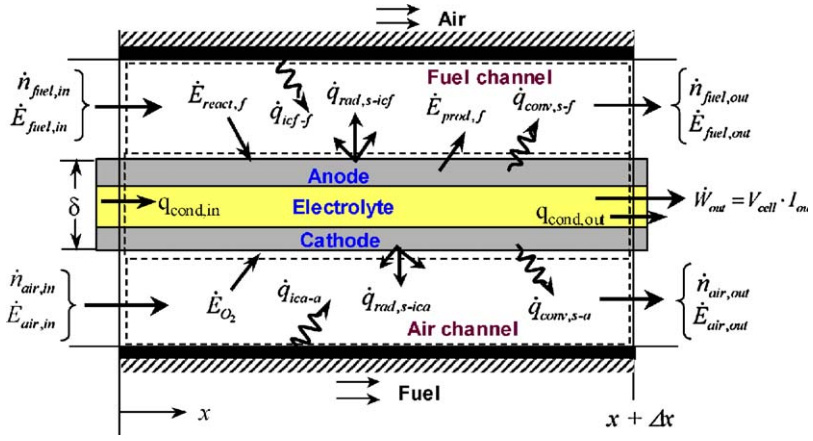

Fig. 1. Axial slice of a cell displaying mass and energy flows.

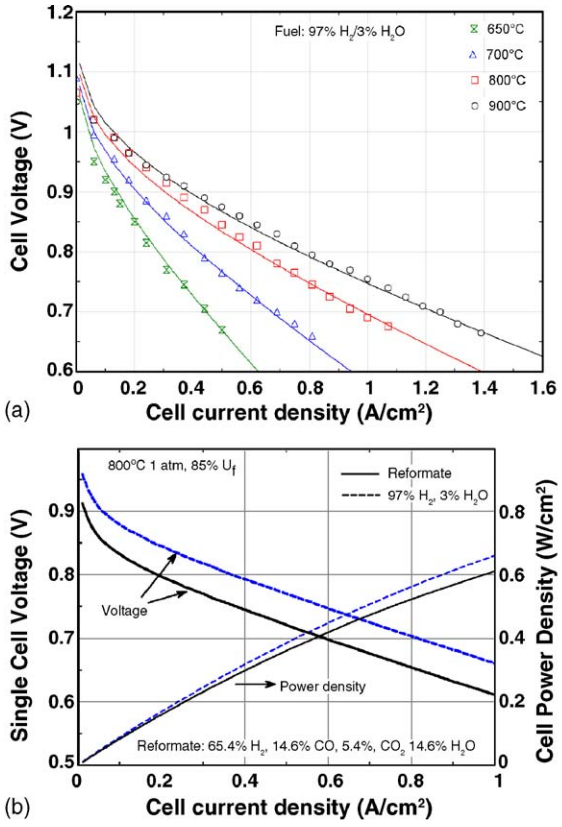

Fig. 2. (a) Experimental voltage–current performance data on hydrogen (b) Model-predicted voltage–current performance on reformate.

3. Performance definitions

SOFC cell-stack efficiency, net system electric efficiency, system cogeneration efficiency, and exergetic system electric efficiency used throughout the present work are defined respectively as,

$$\text{Cell-stack efficiency} \quad \eta_{\text{SOFC}} = \frac{P_{\text{DC}}}{\left(\dot{n}_{\text{fuel,in}}\text{HHV}_{\text{fuel}}\right)_{\text{Anode inlet}}} \tag{2}$$

$$\eta_{\text{sys,e}} = \frac{P_{\text{AC,Net}}}{\left(\dot{n}_{\text{fuel,in}}\text{HHV}_{\text{fuel}}\right)_{\text{system inlet}}} \tag{3}$$

$$\eta_{\text{CHP}} = \frac{P_{\text{AC, Net}} + \dot{Q}_{\text{rec}}}{\left(\dot{n}_{\text{fuel,in}}\text{HHV}_{\text{fuel}}\right)_{\text{system inlet}}} \tag{4}$$

$$\eta_{\text{sys, II}} = \frac{P_{\text{AC, Net}}}{\left(\dot{n}_{\text{fuel,in}}\, a_{\text{fuel}}\right)_{\text{system inlet}}} \tag{5}$$

where P_{DC} is the stack dc power developed, $P_{\text{AC,Net}}$ is the net system AC power, $\dot{Q}_{\text{rec}}$ is the amount of thermal energy from the SOFC system exhaust gas converted to low-grade (60 °C) hot water, $\dot{n}_{\text{fuel, in}}$ is the molar system fuel flowrate, HHV_{fuel} is the fuel higher heating value, and a_{fuel} is the specific exergy of the system fuel input. Thermodynamic property formulations for exergy were employed using methods previously published ([19,20]).

The in-cell fuel utilization refers to the amount of fuel electrochemically oxidized in the anode compartment of the cell-stack and is defined as,

$$U_{\text{f, cell}} = \frac{\left(\dot{n}_{\text{H}_2\text{, consumed}}\right)}{\left(4\dot{n}_{\text{CH}_4} + \dot{n}_{\text{H}_2} + \dot{n}_{\text{CO}}\right)_{\text{anode inlet}}} \tag{6}$$

where $\dot{n}_j$ refers to the molar flow rate of the species of interest. The denominator of Eq. (6) represents the maximum amount of hydrogen that could be supplied with 100% conversion of the reforming and shift reactions. When anode gas recycle is used, the *system* fuel utilization no longer equals the in-cell fuel utilization and must be evaluated at the system fuel input boundary as follows,

$$U_{\text{f, sys}} = \frac{\left(\dot{n}_{\text{H}_2\text{, consumed}}\right)}{\left(4\dot{n}_{\text{CH}_4}\right)_{\text{system feed}}} \tag{7}$$

The amount of stoichiometric air for hydrogen- and methane-fueled systems is calculated using the following respective relations,

$$\lambda_{\text{air,CH}_4} = \frac{\dot{n}_{\text{O}_2\text{,sys}}}{2\dot{n}_{\text{CH}_4\text{,sys}}}; \quad \lambda_{\text{air,H}_2} = \frac{2\dot{n}_{\text{O}_2\text{,sys}}}{\dot{n}_{\text{H}_2\text{,sys}}} \tag{8}$$

where the molar flowrates are taken at the system feed to the plant. The total airflow supplied to the system is greater than the stoichiometric requirements and is determined via energy balances that include the magnitude of the cell polarizations ($E_{\text{N}} - V_{\text{cell}}$, see Eq. (1)), the amount of internal reforming, and the allowable air temperature rise in the cathode.

4. Residential application load profiles

The thermal-to-electric ratio (TER) of a home is the ratio of the thermal energy load to the base electrical demand. A TER may be based on space heating, space cooling, or domestic hot water demands within a residence and its magnitude is highly dependent on location, building type, design, usage patterns, time of day, and time of year. In residential applications, both the timing and magnitude of energy demands vary widely. The annual hourly average domestic hot water TER for a modest (~200 m^2) home in the U.S. can range from 0.7 to 1.0 [21]. The TER for household space heating can be substantially higher (greater than ten times) than that of domestic hot water TERs in northern U.S. climates. Residential-scale fuel cell systems typically generate TERs in the range of 0.5–2 and with the use of thermal storage, can be matched to serve domestic hot water heating loads. The following design studies consider SOFC-CHP systems that produce TERs in the range 0.7–1.0 to be preferred for integration with residential domestic hot water systems.

5. SOFC-CHP system design study

The system model is used to evaluate the performance of different residential-scale SOFC-CHP configurations. More specif-

ically, system flowsheet designs employing the following are discussed[1]:

(a) Hydrogen- and methane-fuels
(b) Fuel gas processing via external and internal reforming of methane (natural gas)
(c) Fuel gas processing via anode recycle
(d) Oxidant gas processing via cathode recycle
(e) Combinations of recycle and extent of internal reforming

Five different system configurations are examined: Case (1) hydrogen-fueled, Case (2) methane-fueled with external and internal catalytic steam reforming, Case (3) methane-fueled with cathode gas recycle (CGR), Case (4) methane-fueled with anode gas recycle (AGR), and Case (5) integration of CGR, AGR, and internal reforming (IR) concepts. The analyses are carried out for a fixed SOFC stack size of 50 cells, each 10 cm × 10 cm, operating at a nominal temperature of 800 °C with a design cell air temperature rise, ΔT_{air}, of 100 °C, 85% system fuel utilization, and a nominal average current density of 0.57 A cm^{-2}. The cell-stack is simulated in a counter-flow configuration as this reactant manifolding scheme enables higher cell efficiency due to higher mean stack temperature and lower internal ohmic resistance [22]. In a counter-flow configuration, the anode exhaust gas can be at a lower temperature and the cathode exhaust gas at a higher temperature than the nominal stack value of 800 °C [7,23]. The current density of 0.57 A cm^{-2} was chosen so that it provided a nominal single-cell voltage of 0.7 V at 85% fuel utilization for the baseline methane-fueled system. In each system configuration, a cell current density of 0.57 A cm^{-2} is specified yielding a fixed fuel energy input to the system rather than a specified system net power output. The conclusions that are drawn from these analyses are independent of whether the fuel input or net power output is specified. Furthermore, sensitivity of the results to selection of different current density and fuel utilization values for the study was investigated, but found not to alter the conclusions reached in the analysis.

Additional system parameters and constraints were set for the analyses. As heat loss to the ambient in small high-temperature systems cannot be neglected, a heat loss term of 3% of the higher heating value of the fuel input was added to the energy balance in the stack periphery. The system exhaust temperature was set to a temperature 25 °C above the dew point of the combustion product gases. The exhaust temperature therefore varied among the system cases. Additionally, the pinch temperature between hot product gases and the water in the boiler was not allowed be lower than 17 °C [11]. A consequence of the boiler pinch temperature constraint is that the location of the boiler in the process gas heat exchanger network may be different and must be selected carefully. In this paper, the boiler is located immediately downstream of the reformer in Case (2a) (see Fig. 5) and between the air preheater and the waste heat recovery hot water heater in all other system configurations (Cases (2b), (2c), (3a), and (3c)) that require a boiler. The reason for this will be discussed in more detail in Section 5.3. Table 1 summarizes the component parameters for the analysis.

Table 1
Summary of system parameters employed in the analysis

Parameter	Value
SOFC stack size	50 cells
Electroactive area	81 cm^2
Current density	0.57 A cm^{-2}
Cell voltage	Variable
Power density	0.40–0.43 W cm^{-2}
Steam-to-carbon ratio	2.0
SOFC fuel utilization	85%
Cathode air temperature rise	100 °C
Nominal cell temperature	800 °C
Air blower efficiency	62.5%
Fuel compressor efficiency	70%
Pump efficiency	60%
Inverter efficiency	92%
Heat loss	3% of fuel input
System exhaust temperature	$T_{dewpt.}$ + 25 °C
Pinch temperature in boiler	≥17 °C

System and performance descriptions for a hydrogen-fueled system (Case 1) are presented first followed by a natural-gas (methane) based system (Case 2a). Incremental performance gains associated with various system configurations are then explored. The design and performance of each system is detailed and a comparative summary of results is provided in Table 2. This section concludes with a performance comparison between hydrogen and methane-fueled systems.

5.1. Hydrogen-fueled SOFC system performance description

Fig. 3 depicts a process flow diagram for a conceptual hydrogen-fueled SOFC system operating near atmospheric pressure with heat recovery (Case 1a) and cathode gas recycle (Case 1b). Process flow data for Case (1b) are also included in this figure. Depending on the method of hydrogen generation and storage, the system may not require a fuel-side compressor, but one is assumed in this configuration. A low-pressure hydrogen-rich fuel mixture (97% H_2 and 3% H_2O) at 15 °C enters the system and is compressed and preheated to 700 °C before admittance to the cell-stack assembly, which operates at a nominal temperature of 800 °C. Air with a stoichiometric ratio of 10.9 enters at station 5 and is preheated to 732 °C before delivery to the cathode compartment of the cell-stack. The SOFC module operating at 0.75 V/cell produces about 2.15 kW of DC power that is inverted to AC. After parasitic power consumption by the air blower and fuel compressor, about 1.5 kW net AC is generated by the system for an overall HHV efficiency of 30.2% (35.7% LHV). Depleted anode gas products exit the stack and catalytically combust resulting in a temperature of 860 °C. The product gas stream is cooled to just above 190 °C by reactant preheat duties. The remaining thermal energy content of the product gas is used to heat water from a temperature of 15–60 °C in the

[1] System design considerations associated with the electrical-side of the plant, such as inverter and power conditioning topologies are discussed further in Braun et al. [21].

Table 2
Performance comparison of various SOFC system design concepts

System concept	Air ratio λ_{air}	Net AC power (kW)	TER ($W_{th}\,W_e^{-1}$)	Air blower power (kW)	Air preheater UA ($W\,K^{-1}$)	Exhaust temperature (°C)	Combustor temperature (°C)	CGR/AGR (%)	SOFC efficiency (% HHV)	System electric efficiency (% HHV)	CHP efficiency (% HHV)
1(a) H_2-fueled	10.9	1.50	1.24	0.47	78.0	54	860	0/0	43.3	30.2	67.6
1(b) H_2-fueled cathode recycle	1.8	1.56	1.37	0.38	0.0	87	978	85/0	42.7	31.4	74.5
2(a) Base Case 0% IR w/boiler	12.5	1.32	0.72	0.53	240.8	51	856	0/0	40.5	34.0	58.5
2(b) 50% IR w/boiler	9.0	1.46	0.62	0.39	79.2	56	854	0/0	45.3	37.6	60.8
2(c) 100% IR w/boiler	5.8	1.58	0.55	0.25	32.1	64	851	0/0	51.4	40.8	63.5
3(a) 0% IR w/cathode recycle	2.1	1.39	0.89	0.43	0.0	83	961	85/0	40.1	35.9	67.8
3(b) 100% IR w/cathode recycle	1.4	1.56	0.71	0.24	0.7	89	981	79/0	50.5	40.2	68.8
4(a) 0% IR w/anode recycle	12.7	1.26	1.23	0.58	142.8	40	853	0/62	32.6	32.7	72.9
4(b) 100% IR w/anode recycle	5.5	1.57	0.87	0.25	25.2	53	852	0/62	39.3	40.6	75.7
5 100% IR w/AGR/CGR	1.5	1.56	0.97	0.23	0.7	77	1008	77/62	38.6	40.2	79.3

heat recovery heat exchanger. Approximately 1.86 kW of low-grade heat (60 °C) in the form of domestic hot water is recovered from the product gas. The system exhausts to the atmosphere at a temperature near 54 °C for an overall cogenerative efficiency of 67.6% (79.9% LHV).

The 50-cell SOFC module operating at 85% fuel utilization generates power with an electric efficiency of 43.3% (51.2% LHV). The substantial stack cooling airflow requirements (and 300 mbar pressurization) results in a 0.47 kW parasitic for the air blower. The system is estimated to reject about 6% of the fuel energy input in the form of heat loss in the inverter and combustor units and approximately 26% of the fuel energy leaves the system accompanying the exhaust gas effluent. In cogeneration mode, a thermal-to-electric ratio of about 1.2 is possible in this configuration.

Fig. 4 displays the energy and exergy flows of the Case (1a) hydrogen-fueled system. Energy values are on a higher heating value basis and exergy values, including irreversibilities within a component, are shown parenthetically. About 5 kW of fuel energy (HHV-basis) enter the system at station 1. In a hydrogen-based SOFC system, fuel processing is typically limited to fuel pressurization and preheat. The 0.36 kW of energy gain in the fuel stream from station 1 to station 3 is primarily due to thermal energy addition by waste heat gases from the catalytic burner. The supply air in the system receives about 0.47 kW of thermal energy from the air blower and another 9.5 kW in the air preheater before delivery to the cell-stack. After power production in the stack, about 1.9 kW of energy remains in the anode exhaust, of which 1.4 kW is chemical energy. In the combustor, the air and depleted anode product gas are mixed to generate 13 kW of thermal energy that serves the process heating needs before heat recovery. The 10 kW of thermal energy exchanged in both reactant preheaters represents nearly seven times the net ac power that is generated from the system. Over 95% of the heat exchange duty in the system occurs in the air preheater and the amount of exergy consumption in the air preheater amounts to 40% of the total in the system. The largest sources of irreversibility in the system are the heat transfer within the air preheater (40%), followed by the heat recovery heat exchanger (14%), and the catalytic combustor (12%). We show in the following section that the use of cathode recycle can be effective at reducing both the magnitude of the heat transfer duty in the air preheater (and thereby, the irreversibilities) and the air blower parasitic power. Details concerning cathode recycle are provided in Section 5.3.3.

5.2. Baseline methane-fueled SOFC system performance description

The 'baseline' design case for this study is a methane-fueled SOFC system (Case 2a) with heat recovery operating near atmospheric pressure with 100% external reforming as shown in Fig. 5. In this configuration, a waste heat boiler provides superheated steam at 5 bar and at a steam-to-carbon ratio of 2:1 for the external reformer. The boiler is located immediately downstream of the fuel reformer to ensure that a sufficient pinch temperature is achieved. Air delivered to the system is preheated to 729 °C

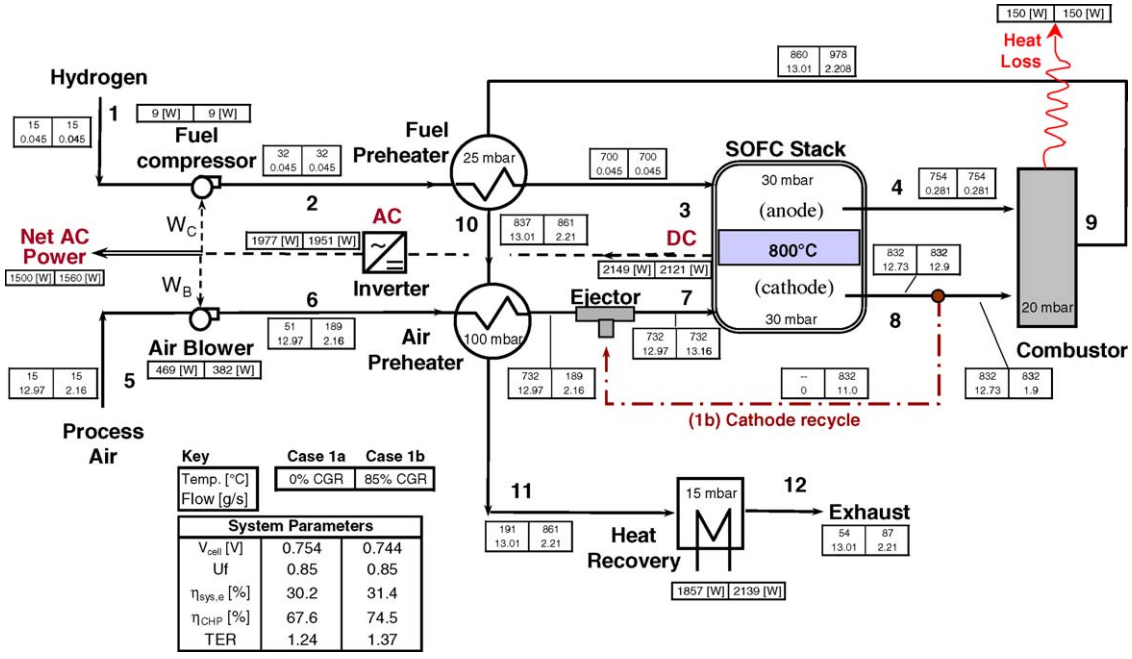

Fig. 3. Process flowsheet of a hydrogen-fueled SOFC system (Case 1a) and CGR (Case 1b).

before delivery to the cathode compartment of the cell-stack. The SOFC module operates at a nominal temperature of 800 °C and 0.705 V/cell to produce 2.0 kW of DC power at a cell-stack efficiency of 40.5% (44.2% LHV). The air blower consumes about 0.53 kW to supply the cooling air at 315 mbar and 1.3 kW net AC power is generated at an overall system HHV efficiency of 34.0% (37.8% LHV). A large fraction of the thermal energy in combusted product gas is required for the fuel processing reactions in the reformer. After the air preheater, the low-grade heat (112 °C) is further cooled to about 51 °C in the hot water heating system to provide 0.95 kW of 60 °C water. The system is capable of an overall cogeneration efficiency of 58.5% (64.9% LHV).

Fig. 6 displays the energy and exergy flows of the Case (2a) natural-gas fueled system. Approximately 3.9 kW of energy in the form of natural gas enters at station 1 and is transformed through mass addition and chemical and thermal energy conversions to nearly 5.6 kW at the anode inlet. The amount of energy supplied to the fuel processing system from the balance-of-plant is approximately 1.7 kW, or about 300% greater than the 0.4 kW required by the hydrogen system of Case (1a) as shown in Fig. 4. About 5 kW of the 5.6 kW of energy delivered to the anode com-

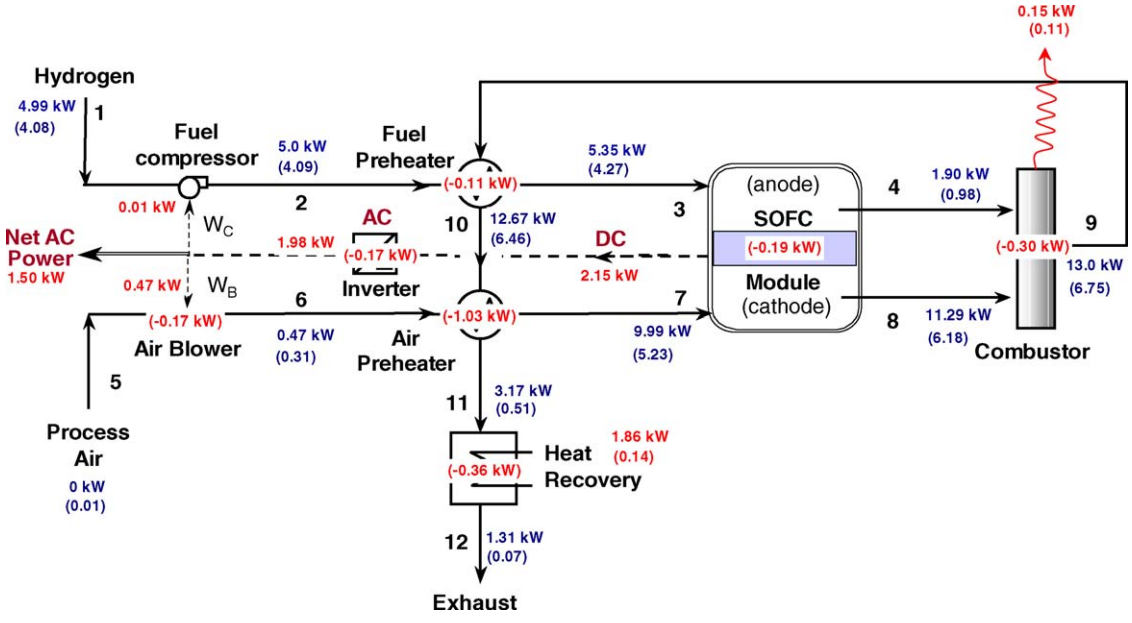

Fig. 4. Energy and exergy (in parentheses) flows in a hydrogen-fueled SOFC-CHP system (Case 1a).

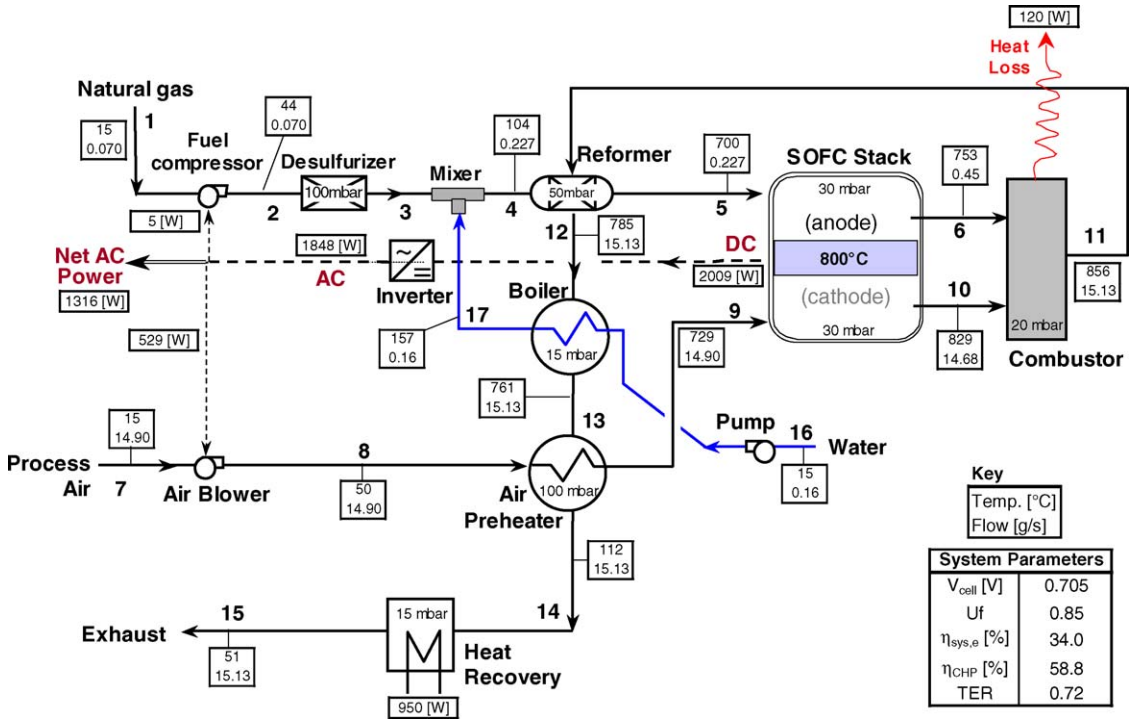

Fig. 5. Process flowsheet of a natural gas-fueled SOFC system with external reforming (Baseline Case 2a).

partment is in the form of chemical energy and the remainder in thermal energy. Thus, the process of fuel reformation using fuel cell product gases serves to increase the magnitude of the chemical energy of the fuel gas stream delivered to the SOFC stack.

The exergy flows of Fig. 6 indicate that the primary system irreversibilities are located in the air preheater (26%), catalytic combustor (19%), boiler (12%), and SOFC stack (11%). The exergy content of the system effluent is less than 3% of the fuel input. Additionally, the exergy content of the delivered hot water

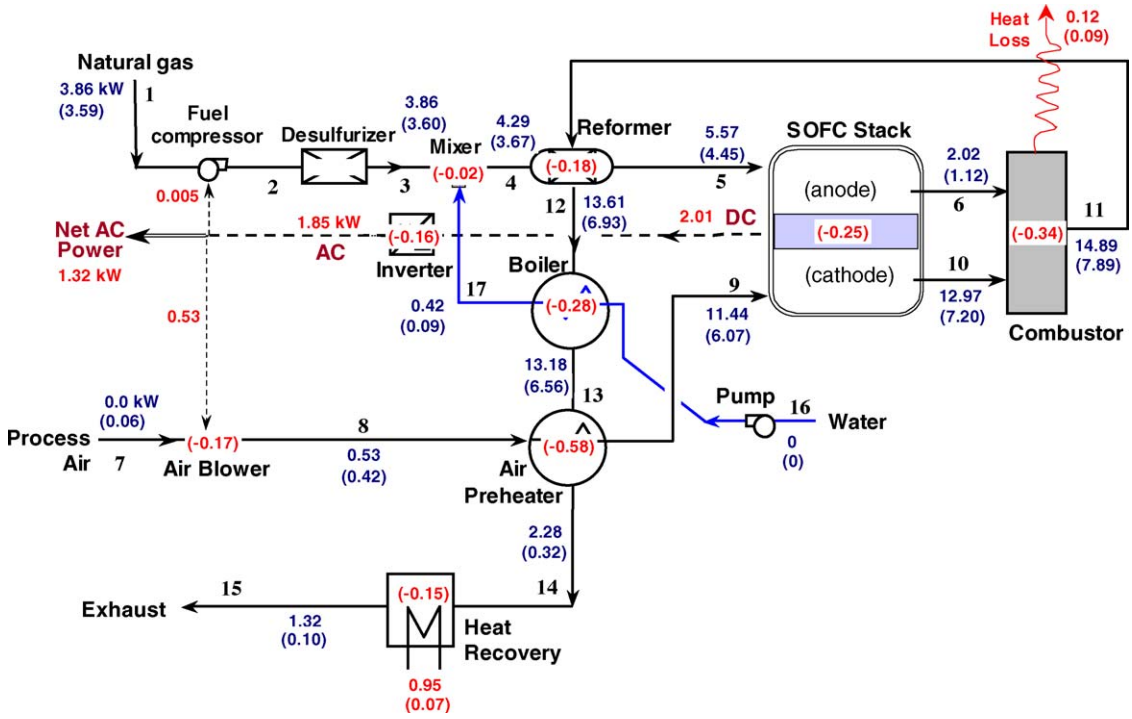

Fig. 6. Energy and exergy (in parentheses) flows in a methane-fueled SOFC-CHP system (Case 2a).

system is only 0.07 kW, compared to the 0.90 kW of thermal energy valuation associated with 60 °C water. Of the 0.43 kW of energy consumed/lost in the combustor, approximately 78% is due to irreversibilities of the combustion process (chemical reaction, thermal energy exchange between reactants and products, and mixing) and 22% through heat transfer to the surroundings. The energy analysis indicates that system improvement efforts should be aimed at reducing the air preheater duty and improving catalytic combustion by reducing the mixing loss.

5.3. Optimal system design configurations

5.3.1. Internal reforming

Locating the reforming process at the anode enables the heat generation associated with the ohmic and activation polarizations to directly serve the endothermic steam reformation reactions; thereby, reducing the cell-stack cooling requirements and the blower parasitic power. There are three main system performance effects associated with internal reforming:

(i) the net system power and efficiency increase with internal reforming due to reductions in parasitic power
(ii) the system TER is reduced due to higher net electric power and lower thermal energy available in the exhaust gas
(iii) capital cost is reduced due to reduction in blower and air preheater capacities and elimination of external reforming hardware

The internal reforming analyses focus on 100% internal reforming within the stack to establish best-case system performance limits; system results for 50% internal reforming, as given in Case (2b), are depicted in Table 2 for reference. The effect of internal reforming (IR) on system efficiency is evident when comparing the values in Table 2 for Cases (2a) and (2c). A system efficiency of 34.0% is achieved in Case (2a) and 40.8% for Case (2c). Both of these cases operate at the same nominal current, temperature, and fuel utilization, employ waste heat boilers for steam reforming and contain no recycle loops. However, as noted in Section 5, the location of the waste heat boiler is downstream of the air preheater in these configurations. An airflow reduction of 54% was obtained with a corresponding decrease of 53% in blower power and nearly 86% in air preheater UA. Approximately 6% of the 86% reduction in air preheater UA is associated with the different boiler location in the heat exchanger network. The 0.28 kW reduction in air blower power is directly transferred as an increase in net system ac power and is the ultimate factor that explains the system performance improvement. Table 2 shows that an increase in the amount of internal reforming results in a decrease of 24% in the system TER. This effect arises from the increased power output while reducing the amount of thermal energy recovery via an increase in the dew point temperature of the exhaust gas stream.

Aside from airflow considerations, the largest effect that the amount of external reforming (or amount of methane conversion in the reformer) has on system design is related to meeting the process heating needs with fuel cell exhaust gases. As the heat required in the external reformer increases with increasing methane conversion (decreasing IR), less thermal energy is available in the fuel cell product gas to serve the other system process needs. In particular, at methane conversions greater than 60%, the pinch temperature in the steam boiler becomes unacceptably low if it is situated downstream of the reformer and air preheater. Thus, the pressure at which steam is generated must be lowered and/or the boiler must be located such that a higher temperature gas source is available to it.

Examining the effect of internal reforming on stack performance is instructive in the proper selection of performance metrics. The stack efficiency obtained by complete external reforming in Case (2a) is lower than that obtained with complete internal reforming (Case (2c)) by nearly 11%. This is a misleading result which is closely associated with the common industry definition of stack efficiency (e.g. [1,24]) defined in Eq. (2). This definition is employed to separate subsystem efficiencies from one another. For instance, to obtain the system electric efficiency using Eq. (2) requires the multiplication of all subsystem efficiencies,

$$\eta_{\mathrm{sys,e}} = \eta_{\mathrm{FPS}}\,\eta_{\mathrm{SOFC}}\,\eta_{\mathrm{PCS}}\,\eta_{\mathrm{mech}} \tag{9}$$

where η_{FPS} is the efficiency of the fuel processing subsystem (FPS), η_{PCS} is the power conditioning system efficiency, and η_{mech} is an efficiency measure of the system ancillary components. Inserting the individual efficiencies in Eq. (9) gives,

$$\eta_{\mathrm{sys,e}} = \underbrace{\frac{\dot{n}_{\mathrm{anode}}\mathrm{HHV}_{\mathrm{anode\ inlet}}}{\dot{n}_{\mathrm{fuel}}\mathrm{HHV}_{\mathrm{system\ inlet}}}\frac{P_{\mathrm{DC}}}{\dot{n}_{\mathrm{anode}}\mathrm{HHV}_{\mathrm{anode\ inlet}}}}_{\text{gross stack efficiency}} \times \underbrace{\frac{P_{\mathrm{AC,Gross}}}{P_{\mathrm{DC}}}\frac{P_{\mathrm{AC,Net}}}{P_{\mathrm{AC,Gross}}}}_{\text{electro-mechanical efficiency}} \tag{10}$$

where $P_{\mathrm{AC,Gross}}$ is the gross ac power after inversion. The first term on the right hand side of Eq. (10) reflects the efficiency of the fuel processing subsystem based on heating values, where the denominator must include any auxiliary fuel supply to the reforming operation. The utility of this metric is questionable as the efficiency often exceeds a value of 1. For instance, the FPS efficiency of the system operation given in Fig. 5 is 128%. The second term in Eq. (10) is the same as defined by Eq. (2) and does not discriminate between cell-stacks that may operate at different fuel utilizations. The first grouping of terms in Eq. (10) produces another common stack efficiency metric, here denoted as the "gross stack" efficiency. This metric does not resolve fuel-processing performance, which is a lumped term. The second grouping in Eq. (10) reflects the "electro-mechanical" efficiency of the plant and the associated impact of parasitic loads.

The fuel reformation process effectively increases the chemical fuel energy content delivered to the stack via the chemical transformations that produce a molar increase in product species. These transformations in the reformer are enabled by the catalyst, the addition of steam, and thermal energy input from the catalytic combustor product gas. The performance metric of Eq. (2) penalizes the SOFC for high-energy content fuel delivered to the anode via the *external* reforming process thereby,

significantly lowering the cell-stack efficiency. The use of the 'gross stack' efficiency metric as given in Eq. (10) registers a 51.9% stack efficiency for Case (2a) and a 51.4% efficiency for Case (2c). This result is in contrast to the nearly 10 point increase in stack efficiency (shown in Table 2) as given by Eq. (2) and is attributable to the change in fuel processing efficiency between the two cases. In fact, neither Eq. (2) nor the 'gross stack' efficiency in Eq. (10) completely assess how effectively the useful energy of the fuel delivered to the stack is utilized. An examination of the exergy consumption (or irreversibility) in the cell-stack provides a more correct approach. A useful definition of the cell-stack exergetic efficiency is,

$$\eta_{\mathrm{II,stack}} = \frac{P_{\mathrm{DC,stack}}}{\dot{A}_{\mathrm{stack,\,inlet}} - \dot{A}_{\mathrm{stack,\,outlet}}} \tag{11}$$

where, $\dot{A}_{\mathrm{stack}}$ is the total exergy entering/exiting the stack accompanying the gas flow at both anode and cathode inlets/outlets. This definition does not penalize the SOFC for the unreacted fuel and thermal energy content in the stack exhaust streams as they may be utilized in downstream components. Instead, it assesses how effective the cell is at producing power based on the net energy content supplied to it from both oxidant and fuel streams. Fig. 7 illustrates the decrease in both the airflow and the exergetic efficiency with increasing amounts of internal reforming. The figure shows that a 2.5% decrease in stack exergetic efficiency occurs when moving from *external* reforming processes to 100% *internal* reforming. The performance decrease, however, is small in comparison to the reduction in parasitic power that is achieved with reduced airflow. Furthermore, these results demonstrate limitations in the ubiquitous use of stack efficiency, as given by Eq. (2), and identify it as a potentially misleading performance metric.

5.3.2. Anode gas recycle (AGR)

Anode exhaust gas recycle is a system concept whereby depleted exhaust gases from the anode outlet are recirculated to the fuel cell inlet providing water vapor in the anode feed gas to assist in methane reformation and inhibit carbon deposition. The recycle of anode exhaust gases also serves to eliminate the waste heat boiler hardware. The amount of AGR is defined on a molar basis as a fraction of the depleted anode exhaust gases,

$$\mathrm{AGR} = \frac{\dot{n}_{\mathrm{recycle}}}{\dot{n}_{\mathrm{anode,\,outlet}}} \tag{12}$$

The amount of anode recycle is typically chosen based on balancing the need for water vapor with the thermodynamic tendency for carbon formation [25]. Estimating the minimum amount of steam required based on evaluation of thermodynamic driving forces results in excessive but "safe" steam-to-carbon ratios of 2 or 3 to 1 [1]. In addition to suppression of coking, the steam-to-carbon ratio also affects the equilibrium yield of hydrogen. As this ratio is increased, the hydrogen yield decreases. Increasing the steam-to-carbon ratio also negatively affects the overall system energy efficiency by requiring additional primary steam generation or recycle of anode effluent for reforming. A steam-to-carbon ratio design point of 2.0 was selected as a reasonable compromise between carbon deposition and hydrogen yield [7].

The system performance using AGR and a system fuel utilization of 85% is reported in Case (4) of Table 2. The primary advantage of anode recycle is the improvement in CHP efficiency from 58.5 to 72.9%. Two effects are responsible for the large gain in CHP efficiency: (i) the increase in thermal energy available for heat recovery due to elimination of the waste heat boiler and (ii) a reduction in water vapor content in the system exhaust gas which enables higher sensible thermal energy recovery.

A gas ejector in which the primary fluid is the fuel and the secondary fluid is the anode exhaust gas is utilized to accomplish the gas recycle. Approximately 62% of the anode exhaust is recycled back to the anode inlet to achieve a steam-to-carbon ratio of 2:1 for reforming. While not considered in this analysis, ejector design and entrainment performance are crucial in achieving the desired steam-to-carbon ratio over the entire range of system operation. Further, it has been shown that the ejector performance itself is strongly influenced by fuel inlet pressure and fuel utilization values [26]. The present analysis focuses on the design point performance alone where the outlet pressure of the ejector is assumed to be equal to the pressure drop in the anode-side of the stack plus the pressure of the secondary flow at the ejector inlet.

The system electric efficiency of Case (4a) is reduced slightly from the base case by 1.2% due to small changes in fuel compressor and blower parasitic power. A *system* fuel utilization of 85% equates to an in-cell fuel utilization of about 69%. Cell-stack efficiency performance is usually enhanced by lower in-cell fuel utilization, but here it is negated by the dilution of H_2 and CO concentrations in the inlet anode feed stream due to the recycle stream [27]. Anode gas recycle improves the CHP efficiency by nearly 15%, largely due to system simplification and a lowering of the exhaust gas dew point. The combination of these effects boosts the TER from 0.72 to 1.23—a value that represents a somewhat higher than necessary TER for typical residential domestic hot water loads. The TER of Case (4a) is also nearly equivalent to that of the hydrogen-based system in Case (1a) while achieving a 2-point higher efficiency. Higher steam-to-

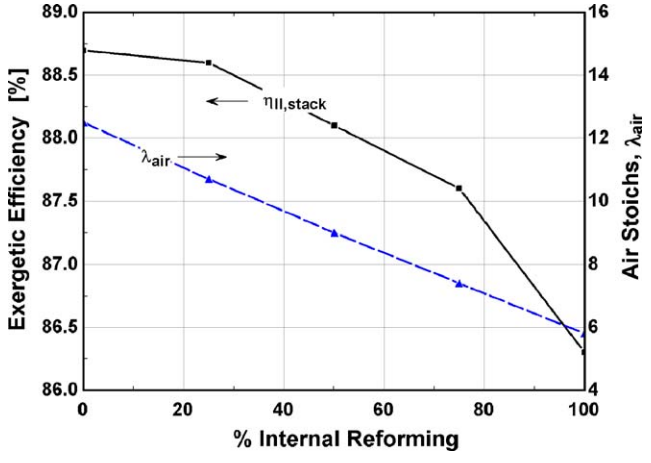

Fig. 7. Effect of internal reforming on the SOFC stack exergetic efficiency.

carbon ratios would reduce the permissible TER of the CHP system.

The stack efficiency of Case (4a) is reduced significantly to 32.6% from that of the baseline system configuration. This reduction arises from the increase in fuel energy delivered to the anode compartment due to recycle of the anode gases. The increase in fuel throughput in the anode compartment effectively lowers the in-cell utilization, but also lowers the stack efficiency per the metric given by Eq. (2).

Case (4b) combines internal reforming with anode gas recycle and the *system* electric efficiency experiences a gain of nearly 8 points over Case (4a) and the CHP efficiency is raised to 75.7% as a result of the reduced cooling airflow and associated parasitic power. Interestingly, the 50% reduction in cooling air flow to the system also reduces the TER by 30%. As will be shown in the next section, Case (4b) efficiency performance is nearly at a maximum and will not be significantly improved with the integration of cathode recycle.

5.3.3. Cathode gas recycle (CGR)

Cathode gas recycle is a system concept where cathode exhaust gases are recirculated to the fuel cell inlet to reduce the size of the air preheater and blower components; thereby, reducing the system cost. CGR also provides an opportunity to enhance system efficiency through a net reduction in the blower parasitic power requirements. In the present study, the amount of cathode gas recycle is defined on a molar basis as,

$$\mathrm{CGR} = \frac{\dot{n}_{\mathrm{recycle}}}{\dot{n}_{\mathrm{cathode,\ outlet}}} \tag{13}$$

Gas ejectors or recycle blowers are used to accomplish the exhaust gas recycle. The effectiveness of CGR concepts in this paper mainly focuses on the use of gas ejectors rather than recycle blowers. A gas ejector pumps a secondary fluid of lower static pressure to higher static pressure via turbulent entrainment and mixing with a high-energy primary fluid. The momentum exchange between the primary and secondary fluids produces a discharge of fluid flow at an intermediate pressure and with higher mass flow. The efficiency of the process can be expressed on an energy basis using the relationship [28],

$$\eta_{\mathrm{ejector}} = \frac{\dot{V}_2}{\dot{V}_1}\frac{P_2 \ln(P_3/P_2)}{(P_1 - P_3)} \tag{14}$$

where $\dot{V}$ is the volumetric flowrate and P is the static pressure at the denoted location in the ejector. The subscripts 1, 2, and 3 refer to the primary driving flow (fresh air), the secondary flow (recycle), and the mixed flow at the ejector outlet, respectively. Using the notation of Eq. (14), the pressure drop in the recycle loop is defined as $P_3 - P_2$. The performance of the ejector device has been simulated using the relationship of Eq. (14), where an ejector efficiency of 20% [26,29] and a 30 mbar pressure drop in the recycle loop are specified for all system case studies.

The simulation results for Case (1b), as shown in Fig. 3 and Table 2, indicate that although a higher discharge pressure is required of the cathode air supply blower, the reduction in system air input (by a factor of 6) is more dominant and creates a net gain in electric efficiency of 1.2% and nearly a 7% gain in CHP efficiency over Case (1a). The system airflow reduction generates an increase in CHP efficiency due to the higher combustor temperature of 978 °C and a larger net thermal energy content in the system exhaust gas, despite the increase in its dew point. Furthermore, the air preheater can be eliminated with 85% recycle of cathode exhaust gases. The CGR concept also produces an improvement of 10% in the thermal-to-electric ratio. Table 2 shows a small decrease in SOFC stack efficiency (0.7%) which results from the dilution of O_2 in the cathode feed gas.

Performance simulations using CGR with ejectors were also carried out on methane-fueled system configurations using either external (Case 3a) or internal reforming processes (Case 3b). A comparison of design Cases (2a) and (3a) show similar trends as that between Cases (1a) and (1b); however, as Table 2 shows, the magnitude of the system performance improvements are slightly larger. System electric efficiency is raised to 35.9% and CHP efficiency to 67.8% for Case (3a). The relatively low CHP efficiency is due to the significant thermal energy required by the fuel processing subsystem for steam generation and reforming of methane, as well as an increase in water content in the stack gas.

Interestingly, the effect of integrating CGR with internal reforming generates a penalty in electric efficiency compared to those systems using internal reforming alone, as in Case (2c). Indeed, a comparison between Case (3b) and (2c) reveals that while airflow reductions are achieved, the blower parasitic is not reduced sufficiently to offset the increased pressure ratio required by the air blower. The dilution of the cathode feed gas from recycle creates a decrease in the SOFC stack efficiency and a concomitant lowering of net system power. Benefits, such as reduced air preheater size, and increased CHP efficiency and thermal-to-electric ratio, are still realized despite a decrease in electric efficiency.

The merit of incorporating cathode recycle using ejector devices is dependent on ejector efficiency and the amount of pressure drop in the recycle loop. Fig. 8 shows the sensitivity of system efficiency and airflow as a function of cathode recycle

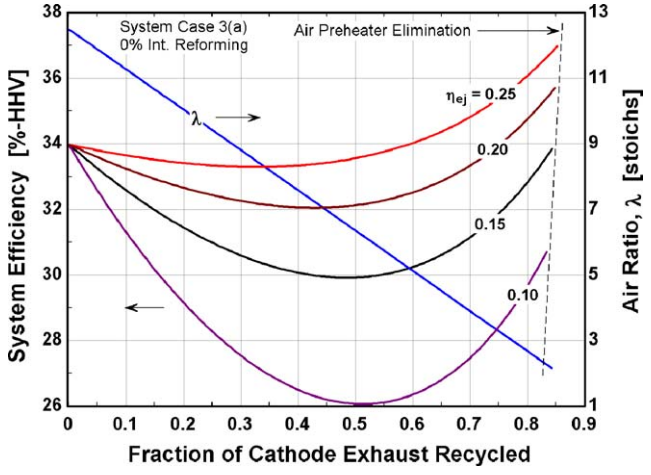

Fig. 8. Sensitivity of system efficiency and airflow to cathode recycle and ejector efficiency.

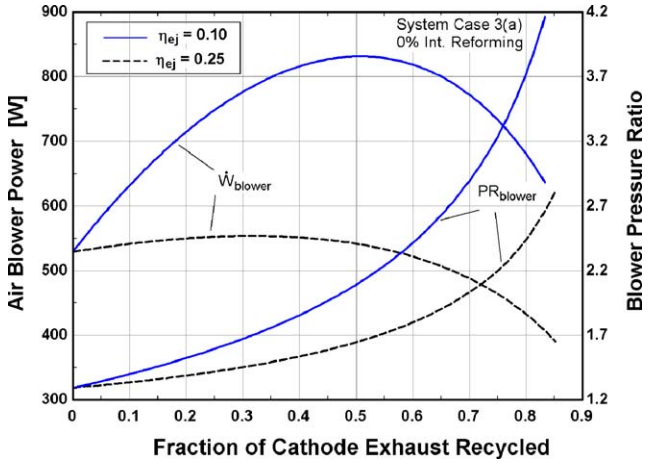

Fig. 9. Effect of Case (3b) cathode recycle on air blower power and blower pressure ratio.

and ejector efficiency. The amount of system airflow, λ, reduces in a linear manner with increasing amounts of cathode gas recycle. The strong effect of ejector efficiency on overall system efficiency is also evident in Fig. 8. At a given ejector efficiency, the reduction in airflow with increasing CGR is negated by the increase in blower pressure ratio required to drive the ejector resulting in a net increase in blower power. This trend continues until an optimum is reached where increases in ejector driving pressure are smaller than the corresponding system airflow reduction. Fig. 9 illustrates this point more clearly at two different ejector efficiencies. The location of maximum blower power corresponds with the minimum system efficiency of Fig. 8.

In practice, the use of a gas ejector can be problematic to implement due to poor controllability of the amount of recycle throughout the operating envelope. Off-design operability may also require a small air preheater to ensure air temperature control at the stack inlet if recycle performance is poor. High temperature recycle blowers are another possible consideration for use in SOFC systems, although the service temperature requirements are severe. Systems incorporating these devices would accomplish much of the same effect as that of an ejector through the reduction of air preheater duty, while still offering reduced overall parasitic power. A simulation of Case (1) using a recycle blower with an isentropic efficiency of 50% was performed and produced a system efficiency of 32.9%. This result is 1.5% improvement in efficiency compared to the ejector performance in Case (1b). The total blower power required for both fresh air supply and cathode gas recycle proved to be about 17% lower than that of an ejector and 33% lower than the non-recycle case. If reliability and efficiency performance of high-temperature recycle blowers can be realized, they offer higher performance than the simpler ejector-based CGR systems. Fig. 8 also shows that if ejector efficiency is 15% or lower, then net improvements in electric efficiency will not be achieved unless the pressure drop in the recycle loop is also substantially lowered. Thus, high ejector efficiency (>15%) and low recycle loop pressure drop (<30 mbar) are desirable system features. Nevertheless, with either recycle blowers or an ejector array, system performance is enhanced through the use of cathode recycle. However, combustor exit temperatures are increased substantially by the reduction in airflow and this effect could alter the system economics by the requirement of higher cost alloy materials in the downstream heat exchangers. The use of expensive metallic alloys could be avoided with the use of cold air injection into the catalytic burner via air bypass from the air blower outlet. Increased system heat loss due to higher combustor temperatures could also mitigate the need for exotic metallic alloys. However, the system cost reductions in air preheater and fresh air blower capacities could be negated with high temperature recycle blowers. This would not be the case with ejectors.

5.3.4. Heat loss in residential-scale SOFC systems

The effect of heat loss in small, high-temperature fuel cell systems can be significant. Heat loss from the SOFC hot module to the ambient has been set to a value equal to 3% of the fuel energy input for the configuration studies presented in Table 2. This amount of heat loss is equivalent to about 150 W for system Case 1(b). In practice, the amount of heat loss will depend on the module geometry/packaging, insulation material and thickness, and the operating temperature of the components within. An estimate of the amount of thermal energy lost from the hot module to the ambient was carried out on a cylindrical vessel containing the cell-stack, air and fuel preheaters, and combustor. A vessel diameter (0.5 m) equal to twice the cell-stack height and a length of 0.6 m were used to estimate the heat transfer area. The temperature within the module was estimated by averaging the nominal cell-stack and the combustor temperatures. The overall UA of the vessel was found to be about 0.541 W K^{-1} using 5 cm of silica aerogel insulation with a thermal conductivity of 0.03 W m^{-1} K. The resulting rate of heat loss for Case 1(b) was estimated at 446 W or 9% of the fuel energy input. Furthermore, the combustor temperature was reduced from 978 to 880 °C which effectively lowers the amount of heat recovery and the corresponding CHP efficiency. Fig. 10 further illustrates how the insulation thickness would affect the magnitude of heat loss and combustor temperature. This first-level calculation reveals that heat loss is indeed significant but is highly variable and design dependent. Additionally, it was found that given an equivalent thermal design of the stack among all systems, the conclusions

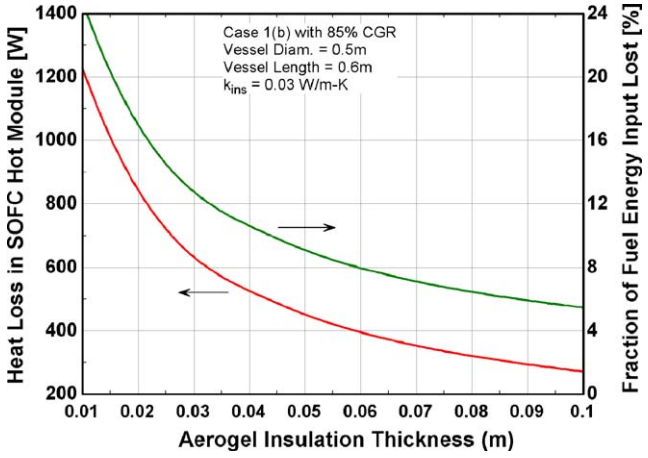

Fig. 10. Sensitivity of heat loss in the SOFC hot module to insulation thickness.

drawn from comparison of different system configurations are not appreciably affected by the magnitude of the heat loss.

5.3.5. Achieving system configurations with maximum efficiency performance

The results displayed in Table 2 illustrate that the highest system efficiencies are achieved with those configurations that involve internal reforming (see Cases (2c), (3b), (4b), and (5)). The greatest efficiency benefit from internal reforming is achieved when 100% of the fuel is converted to hydrogen directly within the cell-stack. Realizing 100% internal reforming in YSZ-based SOFCs is a development effort that faces several challenges. The presence of higher hydrocarbons in the natural gas increases the risk for carbon formation within the cell when internal reforming is desired. The use of a pre-reformer upstream of the fuel cell anode is one approach to reduce the higher hydrocarbons to methane and to generate a small amount of hydrogen in the process. In such a system, the pre-reformer may convert only 15–20% of the fuel to hydrogen; thereby, limiting the amount of internal reforming within the cell-stack to 80–85%. Additionally, the fast kinetics of methane reforming on nickel-based anode cermets creates a strong endothermic cooling effect at the cell inlet thereby increasing the thermally-induced stress of the cell. Anode material and microstructure optimization is required to disperse the amount of methane conversion more uniformly along the streamwise axis of the anode. Thus, in near-term SOFC-based micro-CHP systems, the maximum amount of internal reforming may be limited to near 80%. This limitation reduces the system electric efficiency performance by about 1% from the values listed in Table 2.

It has been shown that internal reforming improves the electric efficiency of the system, but also reduces the TER, a critical parameter in matching residential application requirements. Cases (3) and (4) illustrate that integrating recycling schemes into systems significantly improves TER performance (by 24–29% for CGR and 58–71% for AGR). Fig. 11 depicts the Case (5) flow schematic for a SOFC-CHP system that combines internal reforming, anode recycle (62%) and cathode recycle (77%). Significant system simplification is achieved with the incorporation of these system concepts and Table 2 shows that an electric efficiency of 40.2%, a CHP efficiency of 79.3%, and a TER of 0.97 are achieved. The combustor temperature is high but could be reduced with fresh air bypass from the blower outlet to the combustor inlet. System simplification and reductions in air preheater and air blower capacities suggest lower capital costs can also be realized. A comparison between Case (4b) and Case (5) reveals that the combination of CGR and AGR produces only a slight improvement in TER and CHP efficiency over AGR alone, and lowers the electric efficiency by 0.4%. Given the similar performances of Cases 4(b) and (5), it is difficult to distinguish between the two which design is "optimal". A life cycle cost metric (see [21]) that takes into account both efficiency and cost is preferred to efficiency alone as an optimization parameter. Nevertheless, on a qualitative basis, the small air preheater UA and the 3.6% higher CHP efficiency suggests that Case 5 should offer lower life cycle cost than Case (4b).

5.4. A Performance comparison between hydrogen- and natural gas-fueled systems

Achieving a fair performance comparison between fuel cell systems supplied with different fuel types requires careful selection of efficiency definitions, parameter selection, and system configurations. Numerous bases for comparative assessments between systems can be made, e.g., fixed net power output, fixed current density (i.e., fixed fuel input), fixed system capital cost, etc. In particular, the proper inclusion of energy flows associated with hydrocarbon fuel processing is critical. Furthermore, gaug-

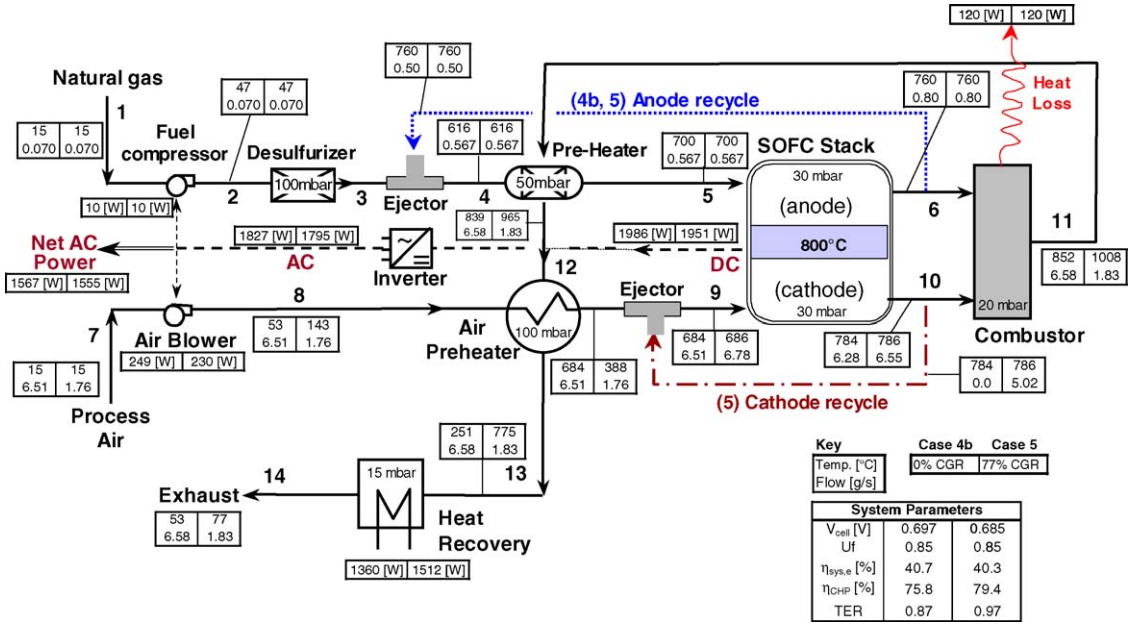

Fig. 11. Process flowsheet diagram of methane-fueled SOFC CHP system with internal reforming and anode and cathode gas recycle (Cases 4b and 5).

ing the relative performance of hydrogen-based versus natural gas-based systems can be complicated by sub-optimal operating point selection. In this section, comparative performance using both fixed net power and fixed current density bases are considered, as well as, a short discussion on the sensitivity of the results to the selection of fuel utilization.

A comparison between system Cases (1a) and (2a) employing a fixed fuel input basis reveals that the hydrogen-based system achieves a lower electric efficiency than the methane-based system (30.2% versus 34.0%) while recuperating more thermal energy. The process diagrams given in Figs. 3 and 5 were generated for systems employing the same operating current density, fuel utilization, cell temperature, and basic process configuration (no recycle loops). A comparison of system performance at a specified current density ensures that the same amount of hydrogen will be electrochemically oxidized within each of the fuel cell stacks. The additional specification of the same fuel utilization ensures that an equivalent amount of hydrogen is supplied to each system. In the methane-fueled system, the amount of hydrogen supplied to the system is determined from the overall methane reforming reaction, $CH_4 + 2H_2O \rightarrow 4H_2 + CO_2$, whereby 4 mol of H_2 are produced for every mole of CH_4 (and 2 mol of water) supplied.

The lower electric efficiency of Case 1(a) when compared to the base case is counterintuitive given that hydrogen is supplied to the system with no penalty for the energy required to produce it. There are several ways to account for this result including the difference in the higher heating values for hydrogen (286 kJ mol^{-1}) and methane (891 kJ mol^{-1}). Thus, the ratio of system fuel energy inputs for hydrogen to methane-fueled systems is then,

$$\left(\frac{\dot{E}_{H_2}}{\dot{E}_{CH_4}}\right)_{\text{system input}} = \frac{\left(\dot{n}_{H_2}\right)\left(\text{HHV}_{H_2}\right)}{\left(\dot{n}_{CH_4}\right)\left(\text{HHV}_{CH_4}\right)} = \frac{(4)(286.0)}{(1)(890.8)} = 1.28 \quad (15)$$

Eq. (15) indicates that, for a given current and fuel utilization, the hydrogen system fuel energy input requires 28% greater energy input as compared to methane-fueled systems. This equation is, essentially, a restatement of the fuel processing subsystem efficiency given in Eq. (10). In practice, hydrogen-fueled SOFC systems are not 28% less efficient than their hydrocarbon-fueled counterparts due to (i) the superior voltage–current performance of SOFCs operating on hydrogen, and (ii) the lower system parasitic power requirements due to lower system pressure drops and required airflow. Both of these effects enable more net power production for the same amount of fuel oxidized (i.e., the same current density). However, the improved cell-stack performance when operating on hydrogen does not entirely offset the larger system fuel energy input, leading to a system efficiency that is lower by nearly 4%. On the other hand, the increase in system fuel energy input and the lack of the energetic needs of a fuel processing subsystem lead to an increase in the amount of thermal energy available for cogeneration, and hence the higher cogeneration efficiency of Case (1a) (67.6% versus 58.5%). More specifically, the methane-based system utilizes high-grade thermal energy from the catalytic burner exhaust to generate additional chemical energy via steam-reforming to supply to the fuel cell stack without incurring a penalty in the system electric efficiency metric. Additional hydrogen is supplied to the system in the form of water, which when combined with methane and thermal energy, boosts the exergetic fuel content fed to the stack and thereby lowers the overall natural gas supply to the system. In contrast, the hydrogen system degrades the high-grade thermal energy content of the exhaust stream to produce *more* low-grade hot water, thereby raising the CHP efficiency, but *lowering* the electric efficiency.

In practice, a hydrogen-fueled SOFC system could operate at a system fuel utilization higher than 85% reducing the useful fuel energy that is allowed to exit the system in the form of low-grade hot water. Higher utilizations can be safely achieved with recycle of the anode tail-gas, however, the recycle dilutes the hydrogen in the anode compartment sufficiently to result in a net reduction in system efficiency. The main advantage of anode recycle in a hydrogen-based system would be to push the system fuel utilization to >95% and thereby eliminate the need for a catalytic combustor while remaining within power plant emission standards and/or code. Nevertheless, if the hydrogen utilization were maximized (without recycle) assuming no concern for stack hardware safety, an optimal system electric efficiency of 32.1% is obtained at 97% utilization. This performance remains nearly 2 efficiency points lower than that of the external reforming natural gas-fueled SOFC system.

Alternate system performance comparisons on the basis of fixed net power (and stack size), rather than fixed current density, were evaluated and are shown in Table 3. The electric efficiency of Case (2a) is reduced to 31.3% by setting the system net power to 1.5 kW. The increase in power from the fixed size cell-stack translates to an increase of the power density to 0.475 W cm^{-2} and a decrease in the single cell voltage to 0.675 V. Nevertheless, this performance is still 1% greater than the hydrogen-fueled system. Increasing the electrochemical fuel utilization improves system efficiency. A fuel utilization (without recycle) of 95% maximizes the system electric efficiency of Case (1a) at 31.3%—a value equivalent to Case (2a). Table 2 also shows the efficiency result when the optimal fuel utilization (90%) is chosen for Case (2a). At 90% fuel utilization, an increase in system electric efficiency to 31.8% is achieved. However, as fuel utilization is increased in external reforming SOFC systems, less thermal energy is available in the fuel cell and burner exhaust gas to serve the other system process needs. In particular, the pinch temperature in the waste heat boiler can become unacceptably low and either the pressure at which steam is generated must be lowered, or other system concepts, such as recycle loops, autothermal reforming, or supplemental fuel firing in the reformer must be employed to accommodate the higher fuel utilization operation.

Other fixed power performance comparisons when releasing the power density constraint also showed higher system efficiencies for the externally reforming methane-fueled system—that is, for all of the comparative performance bases studied, hydrogen systems did not offer any performance advantage or were less efficient.

Table 3
Hydrogen- (Case 1a) and methane-fueled (Case 2a) system performance summaries for fixed power output

System concept	Fuel	Cell voltage (V)	Cell current ($A\,cm^{-2}$)	Power density ($W\,cm^{-2}$)	Fuel utilization	Net AC power (kW)	Electric efficiency (%)
1(a)	H_2	0.754	0.570	0.430	0.85	1.50	30.2
2(a)	CH_4	0.675	0.705	0.475	0.85	1.50	31.3
1(a)	H_2	0.724	0.614	0.444	0.95	1.50	31.3
2(a)	CH_4	0.660	0.735	0.485	0.90	1.50	31.8

6. Summary and conclusions

Design configurations of natural-gas and hydrogen-fueled SOFC-based micro-CHP systems for residential applications have been presented and analyzed. Results for two different hydrogen system configurations and four different natural gas system configurations are presented. The analyses were based on results from thermodynamic models which simulated the efficiency performance of the various system configurations. Two baseline system designs were introduced (1-hydrogen and 1-natural gas fueled) and variations of the system configuration were explored via incorporation of anode recycle, cathode recycle, and internal reforming towards the optimal efficiency. The optimization was subject to cell power density limits and the required domestic hot water TER of residential applications. Optimization of operating parameters such as cell voltage, fuel utilization, amount of internal reforming, etc. for a given configuration were not included, however, sensitivity of the results to a variation in parameters was provided for hydrogen versus natural gas systems.

The results from analysis of the incremental system performance improvements enable several conclusions to be drawn:

1. Hydrogen-fueled SOFC-CHP systems do not offer any electric efficiency advantages over methane-fueled systems despite the "free" supply of H_2 given in the analysis. This result is applicable to both *external* and *internal* reforming SOFC systems and is attributable to the use of thermal energy in the exhaust gas to reform a hydrocarbon fuel such that the net chemical energy of the fuel delivered to the fuel cell stack is increased while the fuel energy feed to the overall system remains lower than hydrogen-based systems despite their superior voltage–current performance. This is an interesting finding and is relevant to analyses where centralized versus distributed hydrogen production facilities in conjunction with SOFC technology are under consideration.
2. Exergy analysis reveals that the largest sources of irreversibility within these systems are contained within the air preheater and catalytic combustor. As the amount of system air input is decreased via recycle loops and internal reforming, the largest source of irreversibility becomes the catalytic combustor.
3. The use of internal reforming in SOFCs reduces system airflow of over 50% and produces the highest system electric efficiency, but CHP efficiency remains relatively low. Exergy analysis demonstrates that stack efficiency performance for internal reformed SOFCs is lower than externally-reformed SOFCs and also reveals limitations in the conventional stack efficiency performance metrics.
4. Cathode gas recycle enhances system efficiency performance by reduction or even elimination of the air preheat duty and the system air input. System TER is also improved by up to 29%. While driving pressures to accomplish the needed amount of recycle with ejectors can more than double the static pressure requirement of the air blower, the net blower parasitic power is reduced because the system air input is lowered by a factor of 6. This reduction of airflow and associated parasitic power translates into increased system power output for the same fuel energy input. However, system electric efficiency improvement is sensitive to ejector efficiency and pressure drop within the recycle loop. Cell-stack efficiency was found to decrease by less than 1% in response to the dilution of O_2 in the cathode compartment.
5. Anode gas recycle was found to be critical to increasing system TER and CHP efficiency performance, but its electric efficiency is quite low without internal reforming. The reduced water vapor content in the exhaust gas is the ultimate factor in enhancing CHP efficiency. Without internal reforming, system electric and stack efficiencies are reduced slightly due to dilution of H_2 and CO concentrations in the anode compartment.
6. The use of anode and cathode gas recycling concepts in combination with internal reforming produces the highest system CHP efficiency and a TER near 1, while minimizing air preheater and air blower capacity requirements.

This paper has focused on developing optimal system configurations that match U.S. residential domestic hot water TERs. SOFC-CHP system design for matching space heating and cooling TERs have not been studied, but are relevant for warmer climates. Strategies for improving the match of TERs of SOFC-CHP systems for residential building applications where the required TER is much greater than 1 are discussed in further detail in Braun et al., [21].

Acknowledgements

The authors would like to thank ASHRAE for a Grant-in-Aid Award to R.J. Braun, the Edwin A. Link Energy Foundation, and the Energy Center of Wisconsin for financial support. Dr. Braun would like to further thank Dr. Sitaram Ramaswamy for helpful discussions.

References

[1] Fuel Cell Handbook, seventh Ed., prepared by EG&G Technical Services, Inc. for the U.S. Department of Energy, Office of Fossil Energy, Morgantown, WV, Contract no. DE-AM26-99FT40575, 2004.

[2] T. Chen, J.D Wright, K. Krist, SOFC Systems Analysis, in: Proceedings of Fifth International Symposium on Solid Oxide Fuel Cells (SOFC-V), PV97-18, Germany, Electrochemical Society, 1997.

[3] E. Riensche, U. Stimming, G. Unverzagt, J. Power Sources 73 (2) (1998) 251–256.

[4] W. Winkler, H. Lorenz, Layout of SOFC-GT Cycles with Electric Efficiencies Over 80%, Proceedings Of the fourth European Solid Oxide Fuel Cell Forum, Lucerne Switzerland, July 10–14, 2002, vol. 1., 2000, pp. 413–420.

[5] W. Winkler, H. Lorenz, J. Power Sources 105 (2002) 222–227.

[6] P. Costamagna, L. Magistri, A.F. Massardo, J. Power Sources 96 (2001) 352–368.

[7] R.J. Braun, Optimal Design and Operation of Solid Oxide Fuel Cell Systems for Small-scale Stationary Applications, Ph.D. Thesis, University of Wisconsin-Madison, 2002.

[8] Exeltech, MX Series product brochure, Fort Worth, TX, www.exeltech.com, 2000.

[9] Engineering Equation Software (EES), F-Chart Software, Middleton, WI, www.fchart.com, 2005.

[10] Conceptual Design of POX/SOFC 5 kW net System, prepared by Arthur D. Little for the Department of Energy, National Energy Technology Laboratory, Morgantown, WV, Final Report, January 2001.

[11] W.L. Lundberg, Solid oxide fuel cell cogeneration system conceptual design, Final Report, GRI-89/0162, Gas Research Institute, Chicago, IL, July 1989.

[12] J.J. Hartvigsen, A.C. Khandkar, Thermally Integrated Reformer for Solid Oxide Fuel Cells, U.S. Patent No. 5,366,819, Washington, DC, November 1994.

[13] E. Achenbach, SOFC Stack Modelling, Final Report of Activity A2, Annex II: Modelling and Evaluation of Advanced Solid Oxide Fuel Cells, International Energy Agency Programme on R, D&D on Advanced Fuel Cells, Juelich, Germany, March 1996.

[14] E. Achenbach, U. Reus, The effect of mass flow distribution on the characteristics of a solid oxide fuel cell system, in: Proceedings of the Sixth International Symp. On SOFCs, (SOFC-VI), PV99-19, The Electrochemical Society, 1999.

[15] T. Ackermann, L.G.J. de Haart, W. Lehnert, F. Thom, Modelling of Mass and Heat Transport in Thick-Substrate Thin-Electrolyte Layer SOFCs, in: Proceedings of the Fourth European SOFC Forum, July, Luzerne, Switzerland, 2000.

[16] E. Achenbach, E. Riensche, J. Power Sources 52 (1994) 283–288.

[17] J.W. Kim, A.V. Virkar, K.Z. Fung, K. Mehta, S.C. Singhal, J. Electrochem. Soc. 146 (1) (1999) 69–78.

[18] D. Ghosh et al., Performance of Anode Supported Planar SOFC Cells, in: Proceedings of the Sixth Int. Symp. on SOFCs (SOFC-VI), PV99-19, The Electrochemical Society, 1999, p.822.

[19] M. Moran, Availability Analysis, ASME press, New York, NY, 1989.

[20] L. Rodriguez, Calculating Available Energy Quantities, in: Second Law Analysis, ACS Symposium Series, vol. 152, The American Chemical Society , New York, NY, 1980.

[21] R.J. Braun, S.A. Klein, D.T. Reindl, Considerations in the design and application of solid oxide fuel cell energy systems in residential markets, ASHRAE Trans. 110 (2004), Part I.

[22] E. Achenbach, J. Power Sources 49 (1994) 333–348.

[23] A. Malandrino, M. Chindemi, Effect of cell configuration and fuel on SOFC modeling, in: Proceedings Of the Third Internat. Symp. On SOFCs, (SOFC-III), PV93-4, The Electrochemical Society, 1993.

[24] L.J. Blomen, M.N. Mugerwa, System design and optimization, in: Fuel Cell Systems, Plenum Press, New York, 1993.

[25] E.S. Wagner, G.F. Froment, "Steam Reforming Analyzed", Hydrocarbon Processing, July 1992.

[26] F. Marsano, L. Magistri, A.F. Massardo, Ejector performance influence on a solid oxide fuel cell anodic recirculation system, J. Power Sources 129 (2004) 216–228.

[27] Y. Yi, A. Rao, J. Brouwer, G.S. Samuelson, J. Power Sources 144 (2005) 67–76.

[28] R.G. Cunningham, R.J. Dopkin, Jet breakup and mixing throat lengths for liquid jet gas pump, Trans. ASME J. Fluids Eng. 96 (1974) 216–226.

[29] C. Garris, W. Hong, C. Mavriplis, J. Shipman, A New Thermally Driven Refrigeration System with Environmental Benefits, in: Proceedings of the 33rd Intersociety Engineering Conference on Energy Conversion, Colorado Springs, CO, August 2–6, 1998.